

Adaptive land classification and new class generation by unsupervised double-stage learning in Poincare sphere space for polarimetric synthetic aperture radars

Yuto Takizawa^a, Fang Shang^b, Akira Hirose^{a,*}

^a Department of Electrical Engineering and Information Systems, The University of Tokyo, 7-3-1 Hongo, Bunkyo-ku, Tokyo 113-8656, Japan

^b Department of Communications Engineering and Informatics, University of Electro-Communications, 1-5-1, Chofugaoka, Chofu, Tokyo 182-8585, Japan

ARTICLE INFO

Article history:

Received 1 July 2016

Revised 4 November 2016

Accepted 8 November 2016

Available online 18 March 2017

Keywords:

Synthetic aperture radar

Polarimetry

Self-organizing map

Geoscience big data

ABSTRACT

Polarimetric satellite-borne synthetic aperture radar (PolSAR) is expected to provide land usage information globally and precisely. In this paper, we propose a unsupervised double-stage learning land state classification system using a self-organizing map (SOM) that utilizes ensemble variation vectors. We find that the Poincare sphere parameters representing the polarization state of scattered wave have specific features of the land state, in particular, in their ensemble variation rather than spatial variation. Experiments demonstrate that the proposed PolSAR double-stage SOM system generate new classes appropriately, resulting in successful fine land classification and/or appropriate new class generation.

© 2017 Elsevier B.V. All rights reserved.

1. Introduction

Satellite-borne synthetic aperture radar (SAR) systems observe the earth continuously, globally and precisely for various purposes [1–12] such as monitoring and mitigation of disaster [13,14], forest biomass estimation for CO₂ reduction, glacier movement watching for water resource protection [15] as well as agricultural crop estimation in the near future. They are also expected to observe various natural and artificial land states. For such purposes, polarimetric SAR (PolSAR) will play an important role in newly launched and future satellite systems [16–23]. In 1990s, some researchers proposed the use of neural networks in PolSAR classification [18]. However, in these years in this field, most of papers deal with decomposition of so-called coherency/correlation matrix, which is the method closest to practical use in present PolSAR automatic land use classification [24,25]. Its basis lies in the linear algebra. However, it sometimes fails in meaningful classification because of its non-uniqueness in the decomposition solution.

Instead of matrix decomposition, we previously proposed the use of Stokes parameters (or Poincare sphere parameters) as the primary variables in the land classification [26]. We also constructed an adaptive classification system based on supervised learning in quaternion domain [27]. With the Stokes representation, the neural classification performance is so high and the

learning cost is so light that its practical application is strongly expected.

Though the supervised learning system shows a high accuracy in its adaptive classification, it does not have the ability to discover new categories of land use. Instead, it indicates uncategorized areas as an undetermined class. Unsupervised learning system may have the ability to discover new classes adaptively. For example, self-organizing map (SOM) with a large number of neurons will generate new classes at appropriate position in the SOM feature space.

In this paper, we propose an unsupervised adaptive method to classify land states using a high-dimensional Poincare-sphere-space self-organizing map that deals with ensemble variation of scattering polarization features. It is a type of quaternion neural networks [28–30], an extended version of complex-valued neural networks (CSOM) [31–36] so that it deals with rotation and amplification/attenuation in three-dimensional feature space of Poincare sphere. In the present case, however, the SOM dynamics include only addition and subtraction without spinor multiplication. Then the basic processing is similar to real-valued high-dimensional SOM. Previously, we reported a preliminary results [37]. In this paper, we newly show its two advantages. One is the auto-generation of new classes. The other is a high spatial resolution revealed with small targets. The latter merit is also compared with supervised learning results.

In the proposal, we employ double-stage clustering to utilize the dispersion features, or ensemble variation features, of pre-

* Corresponding author.

E-mail address: ahirose@ee.t.u-tokyo.ac.jp (A. Hirose).

grouped polarization clusters. In this method, first we extract the scattering feature values as Poincare sphere parameters. Then, we group the pixel parameters locally and finely into clusters. Secondly, we classify the clusters adaptively by using a SOM by taking the ensemble variation of respective clusters into consideration. The preliminary grouping also realizes high robustness against the slant-angle changes in the radar observation to yield useful ensemble variation of the Poincare sphere parameters. It also realizes a high spatial resolution in comparison with the conventional spatial-variation methods.

Experiments to deal with L-band PALSAR 1.1 level data of Advanced Land Observation Satellite (ALOS), Japan Aerospace Exploration Agency (JAXA), demonstrates that the proposed system generates new classes appropriately to represent finer land classification as well as to discover new object classes. These functions will be highly useful in the big-data geoscience era.

2. Poincare sphere parameters: Position vector and variation vector

Fig. 1 shows the observation geometry in a satellite-borne synthetic aperture radar system. It employs the so-called side-looking observation. Full PolSAR system observes 2×2 complex scattering matrix \mathbf{S} at each resolution area. The calculation of Poincare sphere parameters requires to suppose a certain incident wave. The incident wave is expressed by a unit Jones vector $[E_H^i \ E_V^i]^T$ where $(\cdot)^T$ denotes transpose and H, V and i stand for horizontal/vertical polarization and incident wave.

The Jones vector of scattered and received wave $[E_H^r \ E_V^r]^T$ is obtained as

$$\begin{bmatrix} E_H^r \\ E_V^r \end{bmatrix} = \begin{bmatrix} S_{HH} & S_{HV} \\ S_{VH} & S_{VV} \end{bmatrix} \begin{bmatrix} E_H^i \\ E_V^i \end{bmatrix} \quad (1)$$

where E_H^r and E_V^r stand for horizontal and vertical polarization components, respectively. The averaged Stokes vector $[\langle g_0 \rangle \langle g_1 \rangle \langle g_2 \rangle \langle g_3 \rangle]^T$ is then obtained as

$$\begin{bmatrix} \langle g_0 \rangle \\ \langle g_1 \rangle \\ \langle g_2 \rangle \\ \langle g_3 \rangle \end{bmatrix} = \begin{bmatrix} \langle E_H^r E_H^{r*} \rangle + \langle E_V^r E_V^{r*} \rangle \\ \langle E_H^r E_H^{r*} \rangle - \langle E_V^r E_V^{r*} \rangle \\ \langle E_H^r E_V^{r*} \rangle + \langle E_V^r E_H^{r*} \rangle \\ j(\langle E_H^r E_V^{r*} \rangle - \langle E_V^r E_H^{r*} \rangle) \end{bmatrix} \quad (2)$$

where $\langle \cdot \rangle$ denotes spatial or other averaging process and $(\cdot)^*$ means complex conjugate. We define a variable on/in the Poincare sphere \mathbf{P} representing polarization states in three dimension as

$$\mathbf{P} = \left(\frac{\langle g_1 \rangle}{\langle g_0 \rangle}, \frac{\langle g_2 \rangle}{\langle g_0 \rangle}, \frac{\langle g_3 \rangle}{\langle g_0 \rangle} \right) \equiv (x, y, z) \quad (3)$$

We name \mathbf{P} the position vector that represent the position in Poincare space. The norm of \mathbf{P} gives the degree of polarization (DoP) as

$$\text{DoP} = \sqrt{\langle g_1 \rangle^2 + \langle g_2 \rangle^2 + \langle g_3 \rangle^2} / \langle g_0 \rangle \quad (4)$$

The position vector \mathbf{P} is a three dimensional vector relevant to the polarization states of the incident wave. If we consider \mathbf{P}

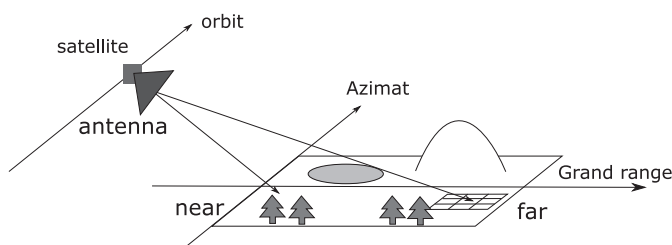


Fig. 1. Satellite-borne SAR observation system and the changes of incidence angles.

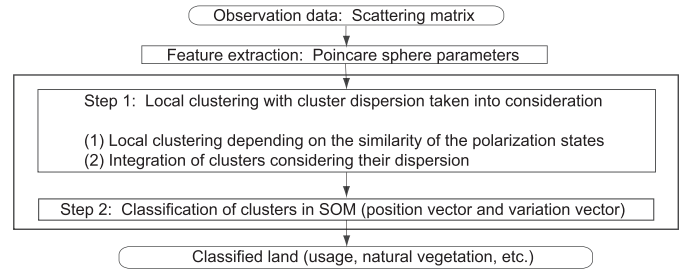


Fig. 2. Total processing flow of the proposed adaptive land state classification system using a SOM in the double-stage learning.

for all the possible incident polarization states, the computational cost will be huge. Instead, we use only important four polarization states, \mathbf{P}_H , \mathbf{P}_V , \mathbf{P}_{45° and \mathbf{P}_{lc} , namely, horizontal, vertical, 45° and left-handed circular polarization [26], as the incident polarization in the following experiments.

3. Adaptive classification by unsupervised double-stage learning

3.1. Overall processing flow

The total process is composed of local clustering in strict condition and unsupervised learning classification of the clusters. **Fig. 2** shows the processing flow in total. A rough description is given here first and then, followed by detailed explanation in the next sections. In this proposal, Step 1 is local clustering to realize the utilization of the variation of Poincare sphere parameters in respective land state clusters in the following process. By regarding a set of position vectors $\mathbf{Q} = [\mathbf{P}_H^T \ \mathbf{P}_{lc}^T \ \mathbf{P}_{45^\circ}^T \ \mathbf{P}_V^T]^T$ as the input vector representing features of each pixel, we conduct the clustering in Step 1 by considering the dispersion of the clusters under construction. We also implement strict clustering with the condition using the dispersion of local clusters.

This local clustering also mitigates the distortion in the radar observation because of the strict condition of local clustering and the order of scanning. As illustrated in **Fig. 1**, a satellite-borne SAR transmits electromagnetic-wave to the earth surface with a slant angle. Hence, the scattered-wave polarization depends on the incident angle [20]. That is, similar land states located near or far range results in polarization states different from one another. This problem mainly arises in the grand range direction. This concern happens also depending on the terrain shape such as slopes and mountains. Therefore, in Step 1 local clustering, we first scan in the azimuth direction, and then proceed line by line in the range direction. Because of this order of scanning and the strict condition of clustering, the pixels far from each other seldom belong to a single cluster, resulting in fine local clusters. Then, we calculate the mean value $\mathbf{Q}(i)$ and the standard deviation $\mathbf{s}(i)$ for ith cluster data.

In Step 2, we classify the clusters adaptively by using SOM. Each cluster has a 24-dimensional feature vector. We found in the following experiments that, even when two areas are located away from each other, common features exist in their parameter distributions corresponding to land states especially in the ensemble variation. Hence, in this process, we multiply the variation by an appropriate weight in order to emphasize its contribution. We describe the details in [Section 3.3](#).

3.2. Local clustering

Step 1 includes the following two processes, i.e. local clustering depending on the similarity of the polarization states and integration of clusters considering their variation.

(1) Local clustering depending on the similarity of the polarization states:

We examine the distances between the scanning center pixel's input vector \mathbf{Q}^c and its surrounding eight pixel vectors \mathbf{Q}^s . We consider the difference of polarization states of scattered waves as sum of the euclidean distances in the four incidence Poincare sphere parameters to calculate distance $D(\mathbf{Q}^c, \mathbf{Q}^s)$ as

$$D(\mathbf{Q}^c, \mathbf{Q}^s) = \|\mathbf{P}_H^c - \mathbf{P}_H^s\| + \|\mathbf{P}_V^c - \mathbf{P}_V^s\| + \|\mathbf{P}_{45}^c - \mathbf{P}_{45}^s\| + \|\mathbf{P}_{135}^c - \mathbf{P}_{135}^s\| \quad (5)$$

If $D(\mathbf{Q}^c, \mathbf{Q}^s)$ is less than a strict threshold D_{th} , which is properly set based on the clustering fitness as explained in Section 4.1, we regard pixels c and s in a single land state cluster.

(2) Integration of clusters considering their variation:

If the input vector of a new pixel labeled a new label is close sufficiently to an existing cluster's mean value $\mathbf{Q}(i)$, the pixel is integrated into the cluster at this time by the process described in the next paragraph. However, in the case that the input vector is away from the center of the existing cluster by the standard deviation or more, it sometimes happens that a cluster j whose land state is actually the same as that of an existing cluster k is generated because of the strict condition.

We integrate them in the every azimuth direction line scanning, namely after the new pixel make a cluster with enough number of pixels and the mean value $\mathbf{Q}(j)$ with them. We use $n(j)$ to represent the number of pixels in cluster j . When $n(j)$ is less than $n(k)$ and the following condition F is fulfilled, we integrate cluster j and cluster k . The condition F is determined based on the standard deviation $us(k)$ where u is a scale. In this process, we change u decreasingly from u_s to u_e according to the increase of $n(k)$ which is a parameter deciding the decreasing speed. That is, we integrate clusters j and k when all the elements of $\mathbf{Q}_{Element}(j)$ are within a distance determined by the standard deviation $us(k)$ from $\mathbf{Q}_{Element}(k)$:

$$F(j, k, u) : |\mathbf{Q}_{Element}(j) - \mathbf{Q}_{Element}(k)| < us_{Element}(k) \quad (\forall Element) \quad (6)$$

$$u = u_e + \frac{u_s - u_e}{1 + n(k)/N} \quad (7)$$

where N is a constant determining the decreasing speed. When a new label is made by a new pixel, it is conducted as $\mathbf{Q}_{Element}(j) = \mathbf{Q}^c$ and $n(j) = 1$ in stricter condition with $F(j, k, u')$ and $u'(u'_s, u'_e)$. The details are given in Section 4.1. With these processes, we can conduct the strict clustering based on the dispersion of Poincare sphere parameters, which is robust against the angle changes of the side-looking satellite observation.

3.3. Adaptive classification by SOM

We define the feature vector of i th clusters as a combination of a set of the position vectors $\mathbf{Q}(i)$ and a set of the variation vectors (standard deviation vectors) $\mathbf{s}(i)$, that is,

$$\mathbf{T}(i) = \begin{bmatrix} \mathbf{Q}(i) \\ \mathbf{s}(i) \end{bmatrix} \quad (8)$$

We use a SOM to classify the clusters suitably based on the feature vectors just like we do in our ground penetrating radar (GPR) systems [36,38,39]. In the present SAR classification system, we choose a 6×6 torus as neuron topology.

Then the input signal is a 24-dimensional feature vector for a cluster $\mathbf{T}^{in}(i)$. We associate neuron g with a weight vector $\mathbf{T}^w(g)$ having the same dimension as that of the input signal. We classify an i th input into a class represented by a neuron g when the

the following distance becomes minimum for g among neuron classes:

$$H(\mathbf{T}^{in}(i), \mathbf{T}^w(g)) = D(\mathbf{Q}(i), \mathbf{Q}^w(g)) + KD(\mathbf{s}^{in}(i), \mathbf{s}^w(g)) \quad (9)$$

where we put an emphasis on the dispersion information in such a way that we first normalize $\mathbf{Q}(i)$ and $\mathbf{s}(i)$, and then multiply normalized $\mathbf{s}(i)$ with an appropriate weight K_0 (i.e., $K = K_0\sigma(\mathbf{Q}(i))/\sigma(\mathbf{s}(i))$). We set the weight K_0 empirically by minimizing the classification error. Self-organization occurs as the updates of the winner $\mathbf{T}^w_{win}(g)$ and the surrounding neurons $\mathbf{T}^w_{neighbor}(g)$ with the sequential signal input. We input the features of $i = 1$ st cluster to $i = I$ th cluster. Then we repeat this process for a sufficient C times. We determine empirically the self-organization coefficients α_0 and β_0 properly to use them varying with the iteration number c as

$$\begin{aligned} \mathbf{T}^w_{win}(t+1) &= \mathbf{T}^w_{win}(t) + \alpha(\mathbf{T}^{in} - \mathbf{T}^w_{win}), \quad \alpha = \alpha_0(1 - c/C), \\ \mathbf{T}^w_{neighbor}(t+1) &= \mathbf{T}^w_{neighbor}(t) + \beta(\mathbf{T}^{in} - \mathbf{T}^w_{neighbor}), \\ \beta &= \beta_0(1 - c/C). \end{aligned} \quad (10)$$

4. Experiments and results

4.1. Observation data and double-stage SOM setup

The observation data used in the following experiment is L-band PALSAR 1.1 level data of ALOS, JAXA, observing the Mt. Fuji area having 2932×1048 pixels. This data is so large and contains much enough kinds of land states in an experiment. We set $N=1000$. The spatial averaging process in (2) is calculated for 5×5 local window.

Fig. 3(a) shows the SOM space structure. It is two-dimensional in torus. We employ a rectangle network so that a winner neuron has four neighbor neurons. **Fig. 3(b)** presents the 6×6 color map corresponding to the above 36 neurons. The color was assigned in such a way that, if two neurons are neighbors to each other, the colors (hue and saturation) are near. Then we can interpret SOM classification results intuitively by looking at the color classification map.

We determined the constants and coefficients introduced in the above process empirically at best values in a series of experiments. Since the distance of each position vectors in a single class is about 0.2 in average, we determined $D_{th}=0.8$ ($= 0.2 \times 4$). We also determined $u_s=3$, $u_e=2$, $u'_s=2$ and $u'_e=1$ and set the maximum and the minimum of the condition F as $F_{min}=0.3$ and $F_{max}=0.5$, while F' as $F'_{min}=0.1$ and $F'_{max}=0.2$, by analyzing quantitatively the position vectors. Step 1 generates about 400 clusters whose populations are 1 – 200,000. Then, in Step 2, the SOM classifies the clusters with $K_0=10.0$, $a_0=0.3$, $b_0=0.04$ and $C=200$.

4.2. Land classification results

Fig. 4 shows the results of various unsupervised classification methods. **Fig. 4(a)** is the result of SOM using only position vectors $\mathbf{Q}(i)$ while (b) is the result using $\mathbf{Q}(i)$ and the spatial variation as we did in Ref. [27], and (c) is the result of the proposal using $\mathbf{T}(i)$, i.e., position vectors $\mathbf{Q}(i)$ and ensemble variation $\mathbf{s}(i)$ as (8). The class colors are synchronized among them in such a manner that the lakes show the same light blue. **Fig. 4(d)** is a Google photo of the observation area with a transform into the same aspect ratio, and (e) is a sketch presenting rough four classes shown in Ref. [27].

Table 1 shows quantitatively the coincidence comparison calculated for 5000 pixels in lake, grass, forest and city areas, respectively. Here, coincidence stands for accuracy in the case of supervised learning. **Fig. 4(d)** shows the numerical evaluation areas of the four land states by white squares. We find that the

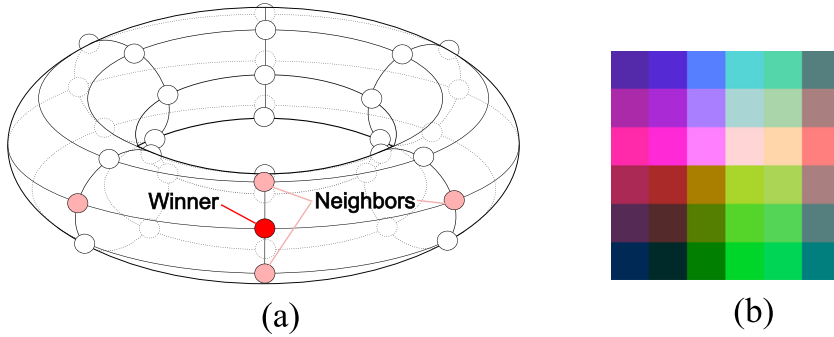


Fig. 3. (a) Torus SOM space and (b) the neuron-label color map. (For interpretation of the references to color in this figure legend, the reader is referred to the web version of this article.)

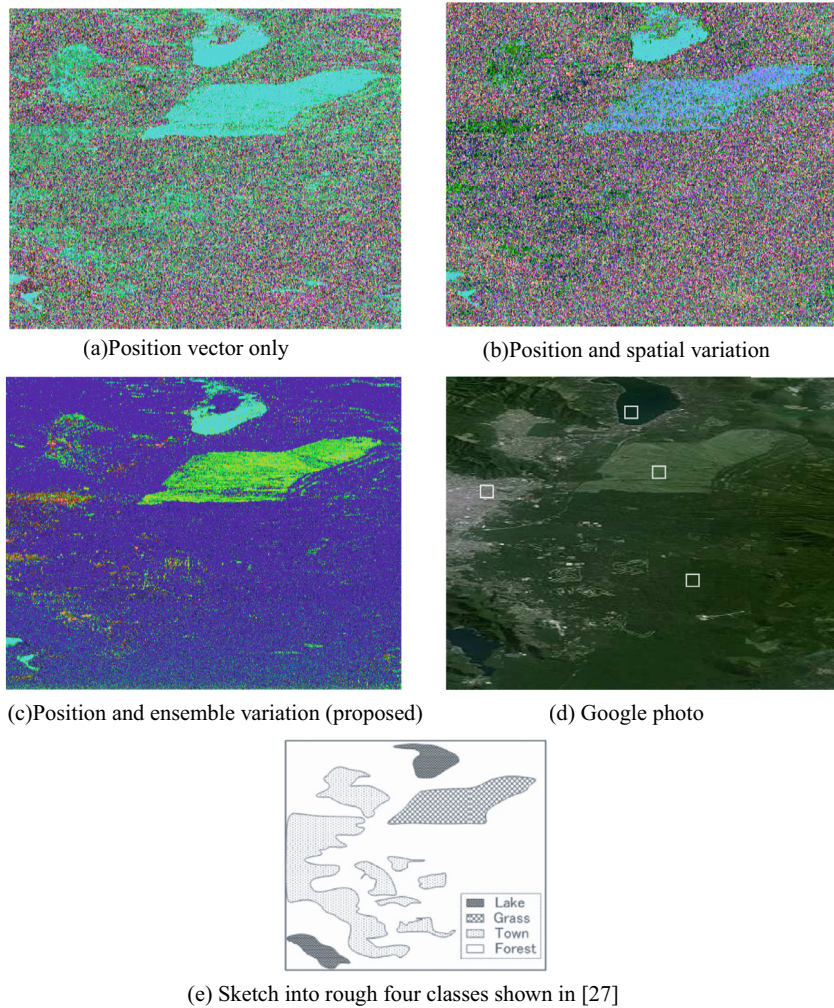


Fig. 4. Land classification results for SOM with (a)position vector only, (b)position vector and spatial variation vector and (c)position vector and ensemble variation vector (proposal), as well as (d)Google optical photo with white squares indicating evaluation areas, and (e)a sketch showing four rough classes after [27].

proposed method achieves the highest overall coincidence. We analyze the details below.

The result using only the position vector in Fig. 4(a) shows a good classification for the lakes, though the lake centers are classified wrongly. This error is attributed to the insensitivity of Poincaré parameters (position vectors and variation vectors) to the wave amplitude because of the normalization in the Stokes vector calculation and the high number (36) of the possible classes. Besides, the large grass area near the big lake is classified to the lake class. The most serious problem is that the large forest area

is classified to various classes. The color distributes widely in the SOM space, showing less meaningful classification. In Fig. 4(b) using spatial variation vector, the classification trend is very similar to (a), though the spatial resolution is apparently lower. However, in the result of proposed method shown in Fig. 4(c), the result is different. The 36 classes are composed of about 7 main classes and other exceptional classes including only a few pixels. The forest areas are classified stably. Town areas include several classes, but are segmented clearly from the forest areas. The results demonstrate that the double-stage SOM method classifies the

Table 1
Unsupervised classification coincidence for the Fujisusono area.

Utilizing	State	Coincidence (%)	Overall Coincidence (%)
(a) No dispersion information	Lake	99.32	37.33
	Grass	0 (96.92% as Lake)	
	Forest	5.06	
	Town	41.86	
(b) Spatial fluctuation	Lake	97.88	51.50
	Grass	64.36	
	Forest	8.98	
	Town	34.78	
(c) Variance in the local clusters	Lake	93.60	83.24
	Grass	74.72	
	Forest	86.60	
	Town	78.02	

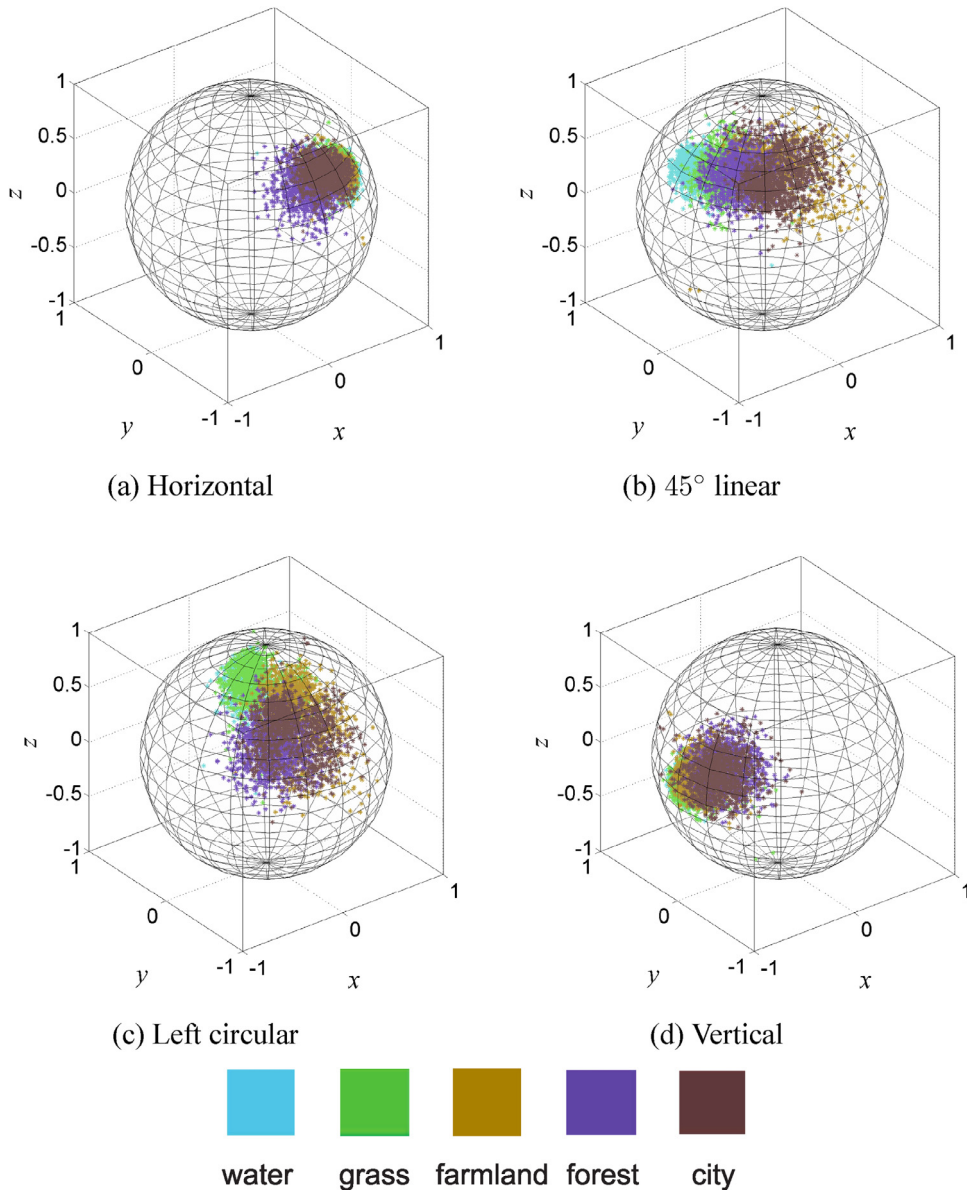


Fig. 5. Position vectors of scattered wave for four polarization states of incident wave, namely, (a)horizontal, (b)45° linear, (c)left circular and (d)vertical polarizations.

polarimetric image adaptively and stably by using the ensemble variation vectors as well as the position vectors.

Fig. 5 plots the position vectors for horizontal, 45° linear, left circular and vertical polarizations corresponding to the major five classes in the result of the proposed method in Fig. 4(c).

The position vectors clearly present distributions different from one another depending on the land states. This fact suggests that the proposed method has the ability to classify the land use adaptively.

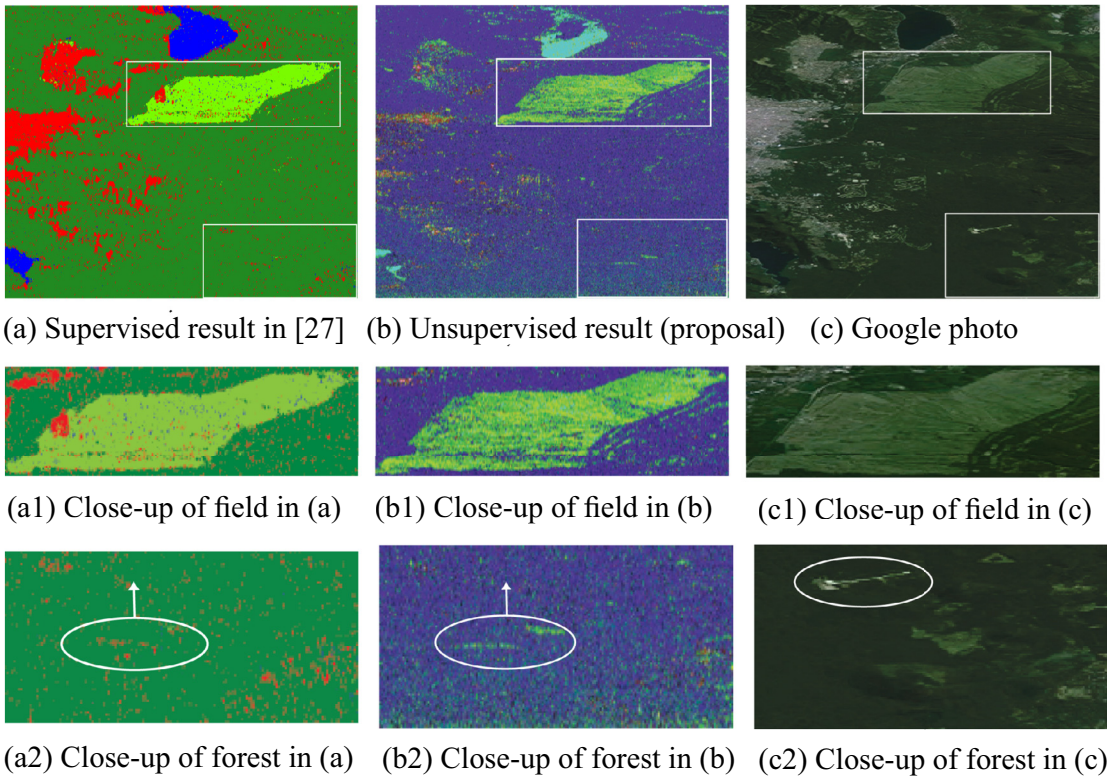


Fig. 6. (a)Result of supervised learning in quaternion neural network [27]. (b)result of the proposed unsupervised double-stage learning and (c)Google photo as well as close-up views for (a1)–(c1) the big grass field and (a2)–(c2) a ski gelaende in a mountainous area, resulting in foreshortening phenomenon in the SAR data. The required location compensation is indicated by the arrows in (a2) and (b2).

4.3. Generation of new classes

The main advantages of the proposed method lie in its ability of new-class generation and high-resolution classification. Fig. 6 compares the proposed SOM unsupervised learning result with the supervised learning result reported in Ref. [27]. Respective images show:

- (a) Supervised learning result to classify the data image into four classes, namely, green: forest, light green: grass, blue: lake, and red: town.
 - (b) Unsupervised learning result to classify the data image into 36 classes in the proposed self-organizing manner, which is identical with Fig. 4(c).
 - (c) Google photo identical with Fig. 4(d).
- (a1) Close-up of a grass area in (a).
 - (b1) Close-up of a grass area in (b).
 - (c1) Close-up of a grass area in (c).
- (a2) Close-up of a forest area in (a). Note that this area is on a so large hill that foreshortening effect causes a shift of the target location. The arrow indicates the original location.
 - (b2) Close-up of a forest area in (b). Note that this area is on a so large hill that foreshortening effect causes a shift of the target location. The arrow indicates the original location.
 - (c2) Close-up of a forest area in (c). No foreshortening effect occurs.

In addition, Fig. 7 is the plots of position vectors for the finer classes appearing in Fig. 7(b1). The distributions for horizontal and vertical incident waves (Fig. 7(a) and (d)) has only a slight dependence on the land state. However, those for 45° and left circular incidence present meaningful dependence. By examining the

ground truth, we have found that the classes correspond to grass, grass with sparse trees, soil-dominant grass and water-covering grass. Accordingly, the rough “grass” in the supervised results can be analyzed and divided into finer classes in the unsupervised learning. The spatial distribution of the classes in Fig. 7(b1) is found corresponding to the land states estimable in (c1). It is found that the unsupervised learning realizes a finer classification successfully.

Fig. 7(b2) includes ski gelaende where the trees are felled. The gelaende location is shifted in the foreshortening effect in comparison with that in (c2) Google photo. The cut down area is so thin that it was not detectable by the previous supervised learning using spatial variation where the resolution is low and the class number was fixed at four. Contrarily, the proposed method used the generated new class appropriately for this extraction. This result also demonstrates the merit of the proposal. Accordingly, we find that the proposed method holds the merits of the new-class generation and the high-resolution classification.

5. Conclusion

We proposed the PolSAR double-stage SOM classification that self-organizingly classifies the Poincare sphere parameters consisting of position vectors and their ensemble variation vectors. Experiments dealing with L-band PALSAR 1.1 level data of ALOS, JAXA, demonstrated that the proposed system classifies land use with a high performance. The main advantages lie in the ability of new-class generation and high-resolution classification. It also mitigates the observation-range and terrain influences on the polarization characteristics. This framework will play an important role in the forthcoming big-data geoscience era.

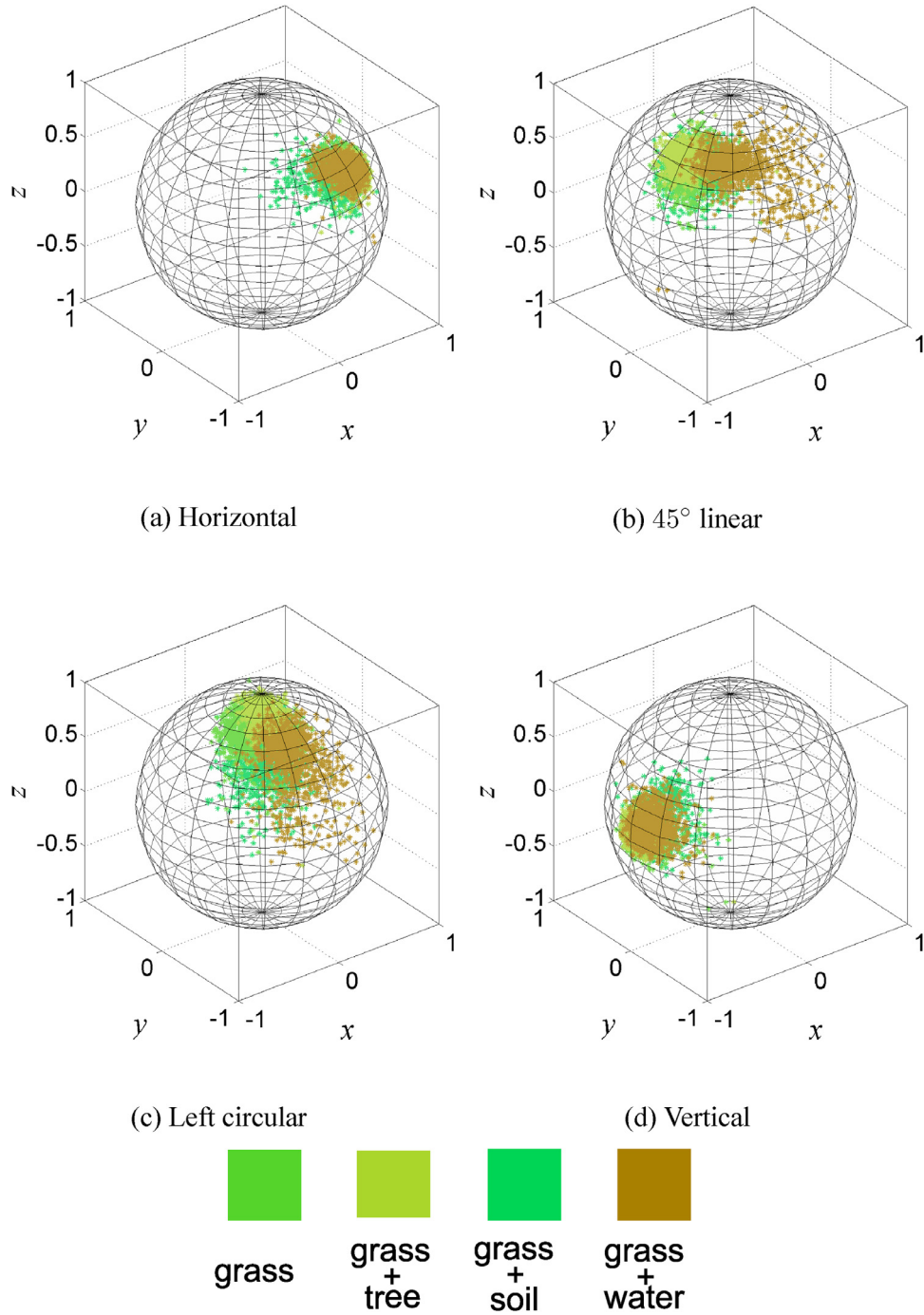


Fig. 7. Position vectors of scattered wave showing fine classes for four polarization states of incident wave, namely, (a) Horizontal, (b) 45° linear, (c) left circular and (d) vertical polarizations.

Acknowledgment

A part of this work was supported by JSPS KAKENHI Grant number 15H02756 and KDDI foundation.

References

- [1] D. Ghiglia, M. Pritt, Two-Dimensional Phase Unwrapping: Theory, Algorithms, and Software, Wiley-Interscience publication, Wiley, 1998.
- [2] M. Pritt, J. Shipman, Least-squares two-dimensional phase unwrapping using FFTs, *IEEE Trans. Geosci. Remote Sens.* 32 (3) (1994) 706–708.
- [3] G. Fornaro, G. Franceschetti, R. Lanari, Interferometric SAR phase unwrapping using Green's formulation, *IEEE Trans. Geosci. Remote Sens.* 34 (3) (1996) 720–727.
- [4] P.A. Rosen, S. Hensley, I.R. Joughin, F.K. Li, S.N. Madsen, E. Rodriguez, R.M. Goldstein, Synthetic aperture radar interferometry, *Proc. IEEE* 88 (3) (2000) 333–382.
- [5] R.M. Goldstein, H.A. Zebker, C.L. Werner, Satellite radar interferometry: two-dimensional phase unwrapping, *Radio Sci.* 23 (1988) 713–720.
- [6] A.B. Suksmono, A. Hirose, Adaptive noise reduction of InSAR image based on complex-valued MRF model and its application to phase unwrapping problem, *IEEE Trans. Geosci. Remote Sens.* 40 (3) (2002) 699–709.
- [7] R. Yamaki, A. Hirose, Singular unit restoration in interferograms based on complex-valued Markov random field model for phase unwrapping, *IEEE Trans. Geosci. Remote Sens.* 6 (1) (2009) 18–22.
- [8] A.B. Suksmono, A. Hirose, Adaptive noise reduction of InSAR images based on a complex-valued MRF model and its application to phase unwrapping problem, *IEEE Trans. Geosci. Remote Sens.* 40 (3) (2002) 699–709. (followed by publisher's errata on Fig. 12)

- [9] J.-S. Lee, W.M. Boerner, D.L. Schuler, T.L. Ainsworth, I. Hajnsek, K.P. Papathanasiou, E. Luneburg, A review of polarimetric SAR algorithms and their applications, *J. Photogramm. Remote Sens.* 9 (2004) 31–80.
- [10] A.B. Suksmono, A. Hirose, Progressive transform-based phase unwrapping utilizing a recursive structure, *IEICE Trans. Commun.* E89-B (3) (2006) 929–936.
- [11] R. Natsuaki, A. Hirose, SPEC method – a fine co-registration method for SAR interferogram, *IEEE Trans. Geosci. Remote Sens.* 49 (1) (2011) 28–37.
- [12] G. Oshiyama, A. Hirose, Distortion reduction in singularity-spreading phase unwrapping with pseudo-continuous spreading and self-clustering active localization, *IEEE J. Sel. Top. Appl. Earth Obs. Remote Sens.* 8 (8) (2015) 3846–3858.
- [13] M. Shimada, JAXA earth observation program digest, *IEEE Geosci. Remote Sens. Mag.* 2 (2) (2014) 47–52.
- [14] R. Natsuaki, A. Hirose, InSAR local co-registration method assisted by shape-from-shading, *IEEE J. Sel. Top. Appl. Earth Obs. Remote Sens.* 6 (2) (2013) 953–959.
- [15] N. Usami, A. Muhuri, A. Bhattacharya, A. Hirose, PolSAR wet snow mapping with incidence angle information, *IEEE Geosci. Remote Sens. Lett.* 13 (12) (2016) 2029–2033.
- [16] W.M. Boerner, Recent advances in extra-wide-band polarimetry, interferometry and polarimetric interferometry in synthetic aperture remote sensing and its applications, *IEE Proc. – Radar Sonar Navig.* 150 (3) (2003) 113–124.
- [17] S.R. Cloude, E. Pottier, An entropy based classification scheme for land applications of polarimetric SAR, *IEEE Trans. Geosci. Remote Sens.* 35 (1997) 68–78.
- [18] K.S. Chen, W.P. Huang, D.H. Tsay, F. Amar, Classification of multifrequency polarimetric SAR imagery using a dynamic learning neural network, *IEEE Trans. Geosci. Remote Sens.* 34 (1996) 814–820.
- [19] R. Touzi, S. Goze, T. Le Toan, A. Lopes, E. Mougin, Polarimetric discriminators for SAR images, *IEEE Trans. Geosci. Remote Sens.* 30 (5) (1992) 973–980.
- [20] F.T. Ulaby, D. Held, M.C. Dobson, K.C. McDonald, T.B.A. Senior, Relating polarization phase difference of SAR signals to scene properties, *IEEE Trans. Geosci. Remote Sens.* GE-25 (1) (1987) 83–92.
- [21] D.L. Evans, T.G. Farr, J.J. van Zyl, H.A. Zebker, Radar polarimetry: analysis tools and applications, *IEEE Trans. Geosci. Remote Sens.* 26 (6) (1988) 774–789.
- [22] R. Touzi, R.K. Raney, F. Charbonneau, On the use of permanent symmetric scatterers for ship characterization, *IEEE Trans. Geosci. Remote Sens.* 42 (10) (2004) 2039–2045.
- [23] R. Shirvany, M. Chabert, J.-Y. Tourneret, Ship and oil-spill detection using the degree of polarization in linear and hybrid/compact Dual-Pol SAR, *IEEE J. Sel. Top. Appl. Earth Obs. Remote Sens.* 5 (3) (2012) 885–892, doi:[10.1109/JSTARS.2012.2182760](https://doi.org/10.1109/JSTARS.2012.2182760).
- [24] Y. Yamaguchi, T. Moriyama, M. Ishido, H. Yamada, Four component scattering model for polarimetric SAR image decomposition, *IEEE Trans. Geosci. Remote Sens.* 43 (8) (2005) 1699–1706.
- [25] G. Singh, G. Venkataraman, Y. Yamaguchi, S.-E. Park, Capability assessment of fully polarimetric ALOS-PALSAR data for discriminating wet snow from other scattering types in mountainous regions, *IEEE Trans. Geosci. Remote Sens.* 52 (2) (2014) 1177–1196.
- [26] F. Shang, A. Hirose, Averaged-Stokes-vector-based polarimetric SAR data interpretation, *IEEE Trans. Geosci. Remote Sens.* 53 (8) (2015) 4536–4547.
- [27] F. Shang, A. Hirose, Quaternion neural-network-based PolSAR land classification in Poincaré-sphere-parameter space, *IEEE Trans. Geosci. Remote Sens.* 52 (9) (2014) 5693–5703.
- [28] N. Matsui, T. Isokawa, H. Kusamichi, F. Peper, H. Nishimura, Quaternion neural network with geometrical operators, *J. Intell. Fuzzy Syst.* 15 (2004) 149–164.
- [29] E. Bayro-Corrochano, *Geometric Computing for Wavelet Transforms, Robot Vision, Learning, Control and Action*, Springer, 2010.
- [30] E.J. Bayro-Corrochano, N. Arana-Daniel, Clifford support vector machines for classification, regression, and recurrence, *IEEE Trans. Neural Netw.* 21 (11) (2010) 1731–1746.
- [31] A. Hirose, S. Yoshida, Generalization characteristics of complex-valued feedforward neural networks in relation to signal coherence, *IEEE Trans. Neural Netw. Learn. Syst.* 23 (2012) 541–551.
- [32] T. Hara, A. Hirose, Plastic mine detecting system using complex-valued self-organizing map that deals with multiple-frequency interferometric images, *Neural Netw.* 17 (8–9) (2004) 1201–1210.
- [33] S. Masuyama, A. Hirose, Walled LTSA array for rapid, high spatial resolution, and phase sensitive imaging to visualize plastic landmines, *IEEE Trans. Geosci. Remote Sens.* 45 (8) (2007) 2536–2543.
- [34] S. Onojima, Y. Arima, A. Hirose, Millimeter-wave security imaging using complex-valued self-organizing map for visualization of moving targets, *Neurocomputing* 134 (2014) 247–253.
- [35] R. Natsuaki, A. Hirose, Circular property of complex-valued correlation learning in CMRF-based filtering for synthetic aperture radar interferometry, *Neurocomputing* 134 (2014) 165–172.
- [36] A. Hirose, *Complex-Valued Neural Networks*, 2nd ed., Springer, Heidelberg, Berlin, New York, 2012.
- [37] Y. Takizawa, F. Shang, A. Hirose, Unsupervised land classification by self-organizing map utilizing the ensemble variance information in satellite-borne polarimetric synthetic aperture radar, in: *Proceedings of the International Conference on Neural Information Processing (ICONIP) 2015 Istanbul*, 2015, pp. 244–252.
- [38] S. Masuyama, K. Yasuda, A. Hirose, Multiple mode selection of walled-LTSA array elements for high resolution imaging to visualize antipersonnel plastic landmines, *IEEE Geosci. Remote Sens. Lett.* 5 (4) (2008) 745–749.
- [39] Y. Nakano, A. Hirose, Adaptive identification of landmine class by evaluating the total degree of conformity of ring-SOM, *Aust. J. Intell. Inf. Process. Syst.* 12 (2010) 23–28.



Yuto Takizawa was born in Nagoya, Japan, on January 16, 1993. He received the B.S. degree in electrical and electronic engineering from the University of Tokyo, Tokyo, Japan, in 2015. He is currently pursuing the M.S. degree. His current research interests include neural networks and complex systems.



Fang Shang received the B.S. and M.S. degrees in electrical engineering and automation from the Harbin Institute of Technology, Harbin, China, in 2009 and 2011, respectively, and the Ph.D. degree in electrical engineering and information systems from The University of Tokyo, Tokyo, Japan, in 2014. She is currently an Assistant Professor with the Graduate School of Informatics and Engineering, University of Electro-Communications, Tokyo, Japan. Her current research interest includes the signal and imaging processing for polarimetric synthetic aperture radar and ultrawideband radar.



Akira Hirose received the Ph.D. degree in electronic engineering from The University of Tokyo, Tokyo, Japan, in 1991. In 1987, he joined the Research Center for Advanced Science and Technology (RCAST), The University of Tokyo, as a Research Associate. In 1991, he was appointed an Instructor at the RCAST. From 1993 to 1995, on leave of absence from The University of Tokyo, he joined the Institute for Neuroinformatics, University of Bonn, Bonn, Germany. From 2006 to 2008, he was also Affiliate Professor of Institute of Space and Astronautical Science (ISAS), Japan Aerospace Exploration Agency (JAXA). He is currently Professor with the Department of Electrical Engineering and Information Systems, The University of Tokyo. The main fields of his research interest are wireless electronics and neural networks. He served as the President of the JNNS, the Vice President of the IEICE Electronics Society, the Editor-in-Chief of the IEICE Transactions on Electronics, an Associate Editor of journals such as the IEEE TRANSACTIONS ON NEURAL NETWORKS and the IEEE GEOSCIENCE AND REMOTE SENSING NEWSLETTER, the Chair of the Neurocomputing Technical Group in the IEICE, the General Chair of the 2013 Asia-Pacific Conference on Synthetic Aperture Radar (APSAR) held in Tsukuba and the General Chair of the 2016 International Conference on Neural Information Processing (ICONIP) held in Kyoto. He currently serves as a member of Aerospace Engineering Committee of JAXA, the Founding Chair of the Complex-Valued Neural Networks Task Force of the IEEE Computational Intelligence Society (CIS) Neural Networks Technical Committee, the Governing Board Member of the Asia-Pacific Neural Network Assembly, the Chair of IEEE GRSS All Japan Chapter, the General Chair of International Geoscience and Remote Sensing Symposium (IGRASS) 2019 Yokohama, an IEEE GRSS Distinguished Lecturer, and the President of Asia-Pacific Neural Network Society (APNNS). Dr. Hirose is a Fellow of IEEE, Senior Member of the Institute of Electronics, Information and Communication Engineers (IEICE) and a member of the Japanese Neural Network Society (JNNS) and APNNS.